

Ambiguities in model-independent partial-wave analysis

F. Krinner,¹ D. Greenwald,¹ D. Ryabchikov,^{1,2} B. Grube,¹ and S. Paul¹

¹*Technische Universität München*

²*IHEP Protvino*

Partial-wave analysis is an important tool for analyzing large data sets in hadronic decays of light and heavy mesons. It commonly relies on the isobar model, which assumes multihadron final states originate from successive two-body decays of well-known undisturbed intermediate states. Recently, analyses of heavy-meson decays and diffractively produced states have attempted to overcome the strong model dependences of the isobar model. These analyses have overlooked that model-independent, or freed-isobar, partial-wave analysis can introduce mathematical ambiguities in results. We show how these ambiguities arise and present general techniques for identifying their presence and for correcting for them. We demonstrate these techniques with specific examples in both heavy-meson decay and pion–proton scattering.

I. INTRODUCTION

In hadron spectroscopy, physicists precisely determine the masses, widths, and other parameters of light mesons and search for new mesonic states, often in very faint signals [16]. In analyzing multibody decays of heavy mesons (for example, B, D, and heavy quarkonia), physicists use spectroscopic techniques to measure both strong and weak phases, allowing for measurement of CP asymmetries.

In a fixed-target scattering experiment, interaction with a target excites an incoming particle into a superposition of states that decays to a set of final-state mesons. All resonant states with quantum numbers allowed by the conservation laws of the initial interaction contribute to the superposition. In heavy meson decay, there is only one decaying state—the heavy meson itself. Both light- and heavy-meson spectroscopy commonly use partial-wave analysis (PWA)—often referred to as Dalitz-plot analysis—which expands the amplitude for the production of the final state into a sum of contributions from partial waves: one for each possible combination of quantum numbers for all states. Each contribution factorizes into components whose forms are dictated by quantum mechanics—spin-dependent amplitudes—and components whose forms are not—dynamic amplitudes, or so-called mass-dependent line shapes. The dynamic amplitudes parameterize the dependence of the partial-wave amplitude on the masses of intermediary states.

Dynamic amplitudes are commonly decomposed into sums of contributions from known resonances. For example, for two pions in a state of spin, parity, and charge-conjugation parity¹ 1^{--} with total isospin 1, the dynamic amplitude can be a sum of contributions from $\rho(770)$ and $\rho'(1450)$. Each resonance has its own dynamic amplitude model—for example the Breit-Wigner line shape—and an accompanying complex constant parameterizing its admixture into the total dynamic amplitude. This de-

composition is commonly called the isobar model, with the individual resonances called isobars.

The results of a partial-wave analysis are strongly dependent on the quality of the analysis model: for example, on the assumptions of what resonances to include; how to model their dynamic amplitudes; and what parameter values to use in those models. PWA with the isobar model suffers other problems: Models quickly become very complicated when we include all possible quantum numbers and all known resonances—even for the production of only three final-state particles. Resonances with identical quantum numbers that significantly overlap in mass—like the $\rho(770)$ and $\rho'(1450)$ —often lead to unphysical modeling. And dynamic amplitude models often ignore the strong interactions that can occur between resonances and other particles in the decay.

These assumptions lead to problems increasingly present in the analyses of the large data sets provided by current and recent experiments. In section II, we present a method to determine dynamic amplitudes directly from the data without models. Several heavy-meson analyses have used this technique in recent years [16–19] and often refer to it as model-independent PWA—we call it *freed-isobar* analysis. We demonstrate its applicability to scattering analyses. In section III, we demonstrate there exist potentially fatal mathematical ambiguities that have not been pointed out in previous analyses. And in section IV, we present several ways to resolve these ambiguities in both heavy-meson and scattering contexts.

II. MODEL-INDEPENDENT PARTIAL-WAVE ANALYSIS

We can remove model dependencies of the isobar model by determining dynamic amplitudes from the data. Instead of decomposing a dynamic amplitude into contributions from intermediary resonances—each with its own dynamic amplitude model—we parameterize it as a complex step function.

Before detailing the formalism of these freed isobars, we briefly review the standard PWA formalism using the isobar model. To make some of the formulas concrete and

¹ We denote these quantum number throughout in this order.

to simplify notation, we refer to the example of three-pion production, from both pion–proton scattering,

$$\pi^- p \rightarrow \pi^- \pi^+ \pi^- p, \quad (1)$$

and D meson decay,

$$D^- \rightarrow \pi^- \pi^+ \pi^-. \quad (2)$$

A fully generic description of the isobar model is available in reference [20].

A. Partial-wave analysis

In partial-wave analysis, we assume events are distributed according to the square of the sum of the partial-wave amplitudes—the intensity of the model. Each amplitude describes a unique transition through intermediary states with well-defined quantum numbers to the final state. We assume the transition proceeds through two-body decays. In our three-pion examples, the quantum numbers defining a partial wave are the spin (J), spin projection (M), parity (P), and charge-conjugation parity (C) of the three-pion system, X ; the spin of the

intermediary two-pion system (S); and the angular momentum (L) between the two-pion system and the third pion, referred to as the spectator pion. Since there are two possible combinations of pions to form the intermediary system, the sum over amplitudes also sums over the two combinations—this is commonly called Bose symmetrization, with each combination referred to as a symmetrization.

Each partial-wave amplitude has a spin-dependent amplitude component, $\psi(m_{3\pi}, \vec{\tau})$, which is dependent on the mass of the initial system, $m_{3\pi}$, and the coordinate in phase space, $\vec{\tau}$, of the final-state particles.² This component is fully specified by the quantum numbers of the wave; but its exact form is formalism dependent.

Each partial wave also has a dynamic amplitude for the production of the wave, $\Delta^{\text{pr}}(m_{3\pi})$, and one for the production of the intermediary state, $\Delta(m_{2\pi})$. Each depends only on the mass of the state whose production it parameterizes—not on any other phase-space coordinates. Commonly, one also includes angular-momentum barrier factors and form factors, which are dependent on both $m_{3\pi}$ and $m_{2\pi}$ —we denote the product of such terms by $F(m_{3\pi}, m_{2\pi})$.

The total amplitude, summing over partial waves, a , and symmetrizations is

$$\mathcal{A}(m_{3\pi}, \vec{\tau}) \equiv \sum_a \Delta_a^{\text{pr}}(m_{3\pi}) \hat{\psi}_a(m_{3\pi}, \vec{\tau}) F_a(m_{3\pi}, \hat{m}_{2\pi}) \Delta_a(\hat{m}_{2\pi}), \quad (3)$$

where we denote symmetrization-dependent functions and variables (and the sum itself) by hats—we use this notation throughout the paper.

For scattering experiments, data are conventionally divided into bins of $m_{3\pi}$ that are analyzed independently, so that the dynamic amplitudes for the production of the three-pion states are learned empirically. In this case, $\Delta_a^{\text{pr}}(m_{3\pi})$ is a set of complex parameters, one for each three-pion mass bin, b —which we call production amplitudes. We rewrite equation (3)—now applying independently for each three-pion mass bin—as a sum over partial waves, each with a production amplitude, $\Delta_a^{(b)}$:

$$\mathcal{A}^{(b)}(\vec{\tau}) \equiv \sum_a \Delta_a^{(b)} \hat{\psi}_a(\vec{\tau}) \Delta_a(\hat{m}_{2\pi}); \quad (4)$$

² For three-particle decay, one needs five independent coordinates to specify $\vec{\tau}$. For scattering, these are usually two Gottfried-Jackson angles [21]; two angles, each one between two final-state momenta; and the invariant mass of one pair of final-state particles. For heavy-meson decay, these are usually two invariant masses of pairs of final-state particles; and three Euler angles describing the overall orientation of the decay plane. If the heavy meson is spinless, as in our example, the Euler angles can be omitted since the decay is isotropic in them.

since within one three-pion mass bin $F(m_{3\pi}, \hat{m}_{2\pi})$ is dependent only on the two-pion mass, we absorb it into $\Delta_a(\hat{m}_{2\pi})$. To simplify notation, since it is sufficient to discuss the formalism within a single three-pion mass bin, we omit the mass-bin index in the remainder of the paper.

In heavy-meson decay, there is only one initial state—the heavy meson itself—with a fixed mass, so we can parameterize $\Delta_a^{\text{pr}}(m_{3\pi})$ by a single complex variable and also use equation (4).

B. Model-dependent isobars

There are many ways to formulate dynamic amplitudes, none of which are dictated by first principles. The most common way is the isobar model, in which the dynamic amplitude for the two-pion state is a sum of contributions from known resonances, ξ , with the quantum numbers of the two-pion state in the wave:

$$\Delta_a(m) = \sum_{\xi} \alpha_{\xi}^a \Delta_{\xi}(m). \quad (5)$$

Each resonance is parameterized by an individual dynamic amplitude, $\Delta_{\xi}(m)$, and a complex admixture vari-

able, α_ξ^a . There are myriad ways to formulate the resonance dynamic amplitudes. One of the most common is the relativistic Breit-Wigner shape:

$$\Delta_\xi^{\text{BW}}(m) \equiv \frac{m_\xi \Gamma_\xi}{m_\xi^2 - m^2 - im_\xi \Gamma_\xi}, \quad (6)$$

which ascribes a mass, m_ξ , and width, Γ_ξ , to the resonance particle.³

We can absorb the production amplitude into the α_ξ , and rewrite equation (4) as a sum over waves and the resonances contributing to each wave:

$$\mathcal{A}(\vec{\tau}) = \sum_a \sum_\xi \hat{\psi}_a(\vec{\tau}) \alpha_\xi^a \Delta_\xi(\hat{m}_{2\pi}), \quad (7)$$

where each complex-valued α_ξ^a parameterizes the production of a resonance and the spectator pion in the total spin configuration of the wave: for example, a three-pion state with quantum numbers 0^{-+} decaying into $f_0\pi^-$ in a relative S wave, where f_0 is a $\pi^-\pi^+$ resonance with quantum numbers 0^{++} and an assumed dynamic amplitude model (and parameter values therein); or a three-pion state with quantum numbers 2^{-+} decaying into $\rho\pi^-$ in a relative P wave, where the ρ is a $\pi^-\pi^+$ resonance with quantum numbers 1^{--} and an assumed dynamic amplitude model.⁴

The isobar model has been very useful in analysis of scattering experiments and heavy-meson decays. But it requires assumptions concerning what resonances are present and what forms their dynamic amplitudes have. These assumptions may bias analyses and ignore small structures not easily modeled, which can distort fit results. These possible substructures—increasingly more visible in the larger and larger data sets of modern experiments—may arise from new resonant states or from final-state interactions.

C. Model-independent isobars

In freed-isobar PWA, we remove the model dependency inherent in the isobar model by parameterizing dynamic amplitudes as complex step functions:

$$\Delta_a(m) = \sum_\beta \omega_\beta^a \mathbb{1}_\beta(m), \quad (8)$$

where the β are disjoint bins of the two-pion mass range; ω_β , the complex values of the dynamic amplitude in those ranges; and $\mathbb{1}_\beta$, the indicator function,

$$\mathbb{1}_\beta(m) \equiv \begin{cases} 1, & \text{if } m \in \beta, \\ 0, & \text{if } m \notin \beta. \end{cases} \quad (9)$$

³ The numerator $m_\xi \Gamma_\xi$ normalizes the shape so that $\Delta_\xi = i$ at $m = m_\xi$.

⁴ States with spin greater than zero should also have a spin projection specified, which we leave off here for brevity.

The division of the mass range into bins is independent for each wave, but is identical for all symmetrizations of a wave. With this model-independent dynamic amplitude, the description of an isobar is freed from assumptions on both what resonances comprise it and how to formulate the dynamic amplitudes of those resonances.

Substituting into equation (4) and absorbing the production amplitude into the ω_β^a , we have

$$\mathcal{A}(\vec{\tau}) = \sum_a \sum_\beta \hat{\psi}_a(\vec{\tau}) \omega_\beta^a \mathbb{1}_\beta(\hat{m}_{2\pi}) \quad (10)$$

This has a form identical to equation (7), with each two-pion mass bin in each wave appearing as an intermediate state with an indicator function for a dynamic amplitude. So we can use the same computational techniques (and software) used for model-dependent PWA.

III. ZERO MODES IN FREED-ISOBAR PWA

If we allow dynamic amplitudes for isobars to have arbitrary forms, mathematical ambiguities may arise: there may exist functions, $\tilde{\Delta}_a$, whose combined amplitude vanishes—

$$\sum_a \hat{\psi}_a(\vec{\tau}) \tilde{\Delta}_a(\hat{m}_{2\pi}) = 0 \quad (11)$$

—no matter what values are taken for parameters of the functions, including an overall scaling of them. Since the amplitude is zero, the parameters of these functions are superfluous degrees of freedom in the total PWA amplitude. We refer to each set of $\tilde{\Delta}_a$ as a zero mode. For such a zero mode to exist, there must be at least two terms in the sum of equation (11); that is, there must be at least two symmetrizations or two waves in the sum.

The binned functions of model-independent PWA introduce enough freedom to the dynamic amplitudes that the sum in equation (11) can be approximately zero—we can have modes that contribute very weakly to the overall amplitude. These weakly contributing modes can complicate analyses and obscure underlying results. Since it is these approximately zero modes that show up in model-independent PWA, we refer to them also simply as zero modes when there is no possibility of confusion.

We can decompose the ω_β^a of equation (10) into a contribution describing nature, α_β^a , and a contribution from zero modes:

$$\omega_\beta^a = \alpha_\beta^a + \sum_z \tilde{\eta}_z z_\beta^a, \quad (12)$$

where each zero mode has complex scaling factor $\tilde{\eta}_z$ and values, z_β^a , in the two-pion mass bins that approximate a $\tilde{\Delta}_a(m)$:

$$\tilde{\Delta}_a^z(m) \approx \tilde{\eta}_z \sum_\beta z_\beta^a \mathbb{1}_\beta(m). \quad (13)$$

Without loss of generality we can define a single zero mode as a collection of real functions with one common complex scaling factor—so that the z_β^a are real.

A. A concrete example

Let us demonstrate the presence of a zero mode in our three-pion examples: The final state particles are all spinless. Let us also consider a spinless three-pion state—which is possible in pion–proton scattering and is always the case in D decay. With the initial-state and final-state particles all spinless, there is only one spin quantum number to consider. Since there are no doubly-charged mesons, we consider only the $\pi^+\pi^-$ intermediary states, of which there are two symmetrizations. We label waves by the spin of the $\pi^+\pi^-$ system; and label the pions as $\pi_1^-\pi_2^+\pi_3^-$ and the two $\pi^+\pi^-$ symmetrizations as 12 and 23.

We will fulfill equation (11) with functions in the S and P waves:

$$\psi_{12}^S(\vec{\tau}) \tilde{\Delta}^S(m_{12}) + \psi_{12}^P(\vec{\tau}) \tilde{\Delta}^P(m_{12}) + \psi_{23}^S(\vec{\tau}) \tilde{\Delta}^S(m_{23}) + \psi_{23}^P(\vec{\tau}) \tilde{\Delta}^P(m_{23}) = 0. \quad (14)$$

The S-wave spin-dependent amplitudes are unity. To find explicit forms for the zero-mode dynamic amplitudes, we must assume a formalism for the P-wave spin-dependent amplitudes. We use the Zemach tensor formalism of [22] because it is simple and common:

$$\psi_{12}^L(\vec{\tau}) = |\vec{p}_1|^L |\vec{p}_3|^L P_L(\hat{p}_1 \cdot \hat{p}_3), \quad (15)$$

where P_L is the L 'th-order Legendre polynomial and the momenta are in the $\pi_1\pi_2$ rest frame. For the P wave,

$$\psi_{12}^P(\vec{\tau}) = \frac{1}{4} (m_{12}^2 + 2m_{23}^2 - m_{3\pi}^2 - 3m_\pi^2); \quad (16)$$

where a and b label waves, β and δ label two-pion-mass bins in each, respectively, and the sums are over possible symmetrizations of each wave. The normalization constants

$$\mathcal{N}_{a\beta}^2 \equiv \int \left| \sum \hat{\psi}_a(\vec{\tau}) \mathbb{1}_\beta(\hat{m}) \right|^2 d\vec{\tau}, \quad (21)$$

are chosen such that the diagonal elements of the matrix are unity. They mitigate spurious effects from two-pion mass bins that hang over an edge of phase space. It is enlightening to connect this mathematical tool back to a physical interpretation: This is the overlap integral matrix for our two-pion mass bins. An eigenvector of it

ψ_{23}^P is formed by swapping m_{12} and m_{23} . If we set $\tilde{\Delta}^P(m)$ constant, then the P-wave contribution in equation (14) has terms that are either independent of the two-pion masses or dependent on only one two-pion mass—that is, there are no terms dependent on both m_{12} and m_{23} . We can cancel all these terms with the S-wave dynamic amplitude. The explicit zero-mode dynamic amplitudes are

$$\tilde{\Delta}^P(m) = 4\tilde{\eta} \quad (17)$$

$$\tilde{\Delta}^S(m) = \tilde{\eta}(m_{3\pi}^2 + 3m_\pi^2 - 3m^2). \quad (18)$$

The zero mode has two degrees of freedom, those of the arbitrary complex coefficient $\tilde{\eta}$.

In the appendix, we give a fuller picture of zero modes in the decay of a spinless particle to three spinless particles and show an example of a zero mode contained entirely in one freed amplitude in a spinful decay.

B. Numerically determining zero modes

Most zero modes are not as simple as the example above. Those for higher-spin decays are particularly more complicated. But we can numerically determine their shapes in the freed-isobar formulation.

In model-independent PWA, a zero mode satisfies

$$\sum_{a,\beta} \hat{\psi}_a(\vec{\tau}) z_\beta^a \mathbb{1}_\beta(\hat{m}_{2\pi}) \approx 0, \quad (19)$$

where the z_β^a are the values in each two-pion mass bin of each freed wave such that the sum is very small—they are real since we have defined a zero mode as real in equation (13). The standard mathematical tool to solve for the z_β^a that fulfill equation (19) is to look for the eigenvectors of the Gram matrix of the freed isobars that have vanishingly small eigenvalues. This matrix is

$$\mathbf{I}_{a\beta,b\delta} \equiv \frac{1}{\mathcal{N}_{a\beta} \mathcal{N}_{b\delta}} \int \left(\sum \hat{\psi}_a^*(\vec{\tau}) \mathbb{1}_\beta(\hat{m}_{2\pi}) \right) \left(\sum \hat{\psi}_b(\vec{\tau}) \mathbb{1}_\delta(\hat{m}_{2\pi}) \right) d\vec{\tau} \quad (20)$$

with a very small eigenvalue is a set of dynamic amplitude values in each bin of each wave that contribute negligibly to the overall intensity. The set of freed-isobar dynamic amplitudes forming a zero mode are therefore

$$\tilde{\Delta}_a^z(m) = \tilde{\eta}_z \sum_\beta z_\beta^a \mathbb{1}_\beta(m), \quad z_\beta^a \equiv \tilde{z}_\beta^a \mathcal{N}_{a\beta}^{-1} \quad (22)$$

where \tilde{z}_β^a are the elements of the eigenvector.

We use numerical integration techniques to construct the overlap-integral matrix. It will have $\dim(\mathbf{I})$ eigenvectors. Those corresponding to zero modes will not only be small, but will have values that decrease quadratically

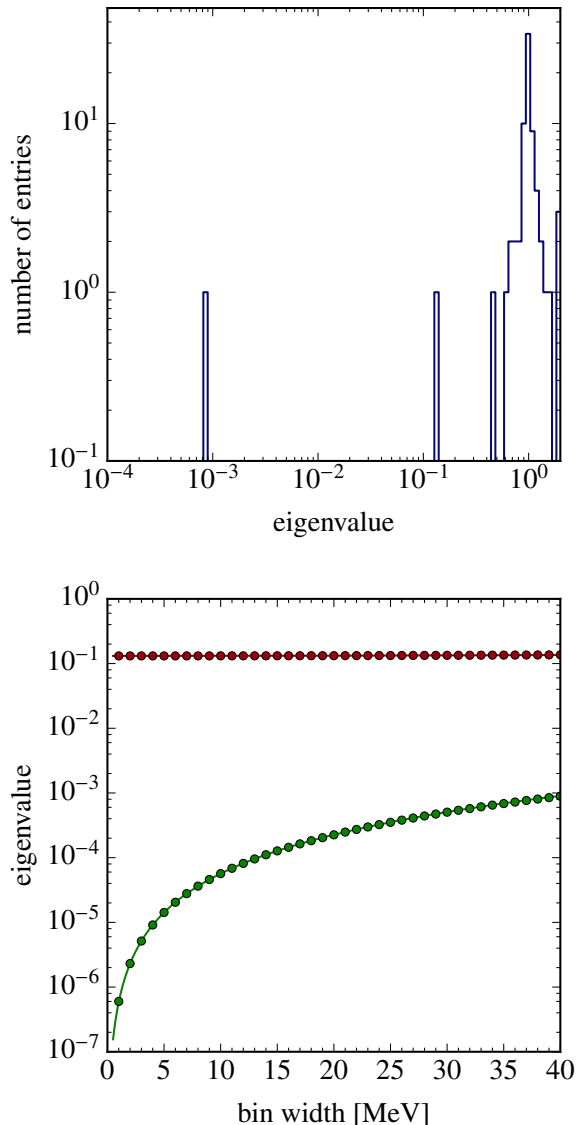


FIG. 1: Eigenvalue spectrum (top) of the integral matrix for freed S and P waves in $D^- \rightarrow \pi^- \pi^+ \pi^-$; and the mass dependence of the two smallest eigenvalues (bottom).

with the (average) width of the two-pion-mass bins, owing to the construction of the Gram matrix.

We demonstrate this technique with the decay $D^- \rightarrow \pi^- \pi^+ \pi^-$ with the S and P waves freed. We expect to find the zero mode of equations (17) and (18). The top plot in figure 1 shows the eigenvalue spectrum of the integral matrix. There is one significantly small eigenvalue. The bottom plot in the figure shows the dependence of this eigenvalue and the next-largest one on the average bin width. The smallest eigenvalue quadratically depends on the bin width, but the next-largest one is constant. Figure 2 shows the zero mode formed from the eigenvector alongside that of equations (17) and (18)—

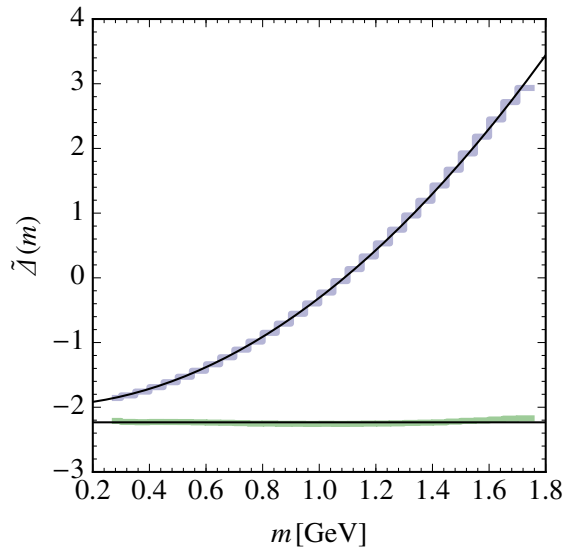


FIG. 2: Components of the numerically determined zero mode for freed S (blue) and P (green) waves in $D^- \rightarrow \pi^- \pi^+ \pi^-$ and the zero mode of equations (17) and (18) (black).

the two are nearly indistinguishable⁵. They deviate from each other only in the P-wave high-mass region: The S-wave analytical zero mode varies most rapidly at high masses, so the step function is a worse approximation there than it is at low masses. The P-wave step function at high mass deviates from the expected form to compensate for the discrepancy in the S wave. When we reduce the bin widths, this discrepancy disappears.

IV. RESOLVING ZERO-MODE AMBIGUITIES

When we fit a freed-isobar PWA model to data, zero modes will contribute to the dynamic amplitudes the fitter finds—the ω_β^a of equation (10)—with their complex $\tilde{\eta}_z$ taking on arbitrary values as artifacts of the fitting process. We can correct for their presence using knowledge of their shapes and some assumption about the true underlying amplitudes and recover the underlying physical values, the α_β^a , that are the goal of an analysis. We refer to the fit that determines the ω_β^a as the fit to data and further steps (including additional fits) that determine the α_β^a as the zero-mode correction.

There are many possible assumptions we can make about the true underlying physical amplitudes; we present three examples below, which each assumes a

⁵ The shapes of the zero mode also include barrier factors and form factors. If these are put into an analysis model explicitly, the shapes of the zero mode change accordingly.

model for some part of the freed isobar amplitudes. This gives us expectations for the underlying physical values, which we label ϵ_β^a . Equation (12) tells us that the difference between the underlying value and our expectation

is

$$\alpha_\beta^a - \epsilon_\beta^a = \omega_\beta^a - \sum_z \tilde{\eta}_z z_\beta^a - \epsilon_\beta^a; \quad (23)$$

since we can learn the z_β^a using the method described in section III B, the only unknowns are the $\tilde{\eta}_z$. We can fit for the $\tilde{\eta}_z$ and correct for them, yielding the true underlying values. We do this by minimizing

$$\chi^2 \equiv \sum_{a\beta, b\delta} \left(\omega_\beta^a - \sum_z \tilde{\eta}_z z_\beta^a - \epsilon_\beta^a \right) C_{a\beta, b\delta}^{-1} \left(\omega_\delta^b - \sum_z \tilde{\eta}_z z_\delta^b - \epsilon_\delta^b \right), \quad (24)$$

where a , β , b , and δ are as defined for equation (20) and $C_{a\beta, b\delta}$ is the matrix of covariances of the ω_β^a determined by the fit to data.

This step is not equivalent to having assumed a model from the very start: The model-independent approach has many more degrees of freedom than model-dependent approaches. The zero-mode correction step only reduces the number of degrees of freedom in the analysis by the number of free parameters in equation (24), leaving still much more freedom than in a model-dependent analysis.

A. Zero-mode correction examples

We demonstrate zero-mode correction using simulated data of three-pion states produced by D-meson decay and pion-proton scattering. We test three types of assumptions to correct for the zero mode: a model that predicts a value in every two-pion-mass bin in every freed wave with the $\tilde{\eta}_z$ the only free parameters; a model for only a subset of bins, with the $\tilde{\eta}_z$ the only free parameters; and a model with additional free parameters beyond those of the zero mode.

For $D \rightarrow \pi^- \pi^+ \pi^-$, we generated one million events according to a model containing $f_0(980)\pi^-$ in the S wave and $\rho(770)\pi^-$ in the P wave, with both resonances modeled by the relativistic Breit-Wigner lineshape [23]. For the spin-dependent amplitudes, we used the Zemach formalism of [22].

Our D-decay fit model frees both the S and P waves. The steps in both freed waves are contiguous and cover the full mass range from $2m_\pi$ to $m_D - m_\pi$; they are 20 MeV wide. With freed S and P waves, as we demonstrated above, there will be a zero mode with one complex degree of freedom.

For $\pi^- p \rightarrow \pi^- \pi^+ \pi^- p$, we generated 260,000 events in the three-pion mass range from 1.50 GeV to 1.54 GeV according to the model used by the COMPASS collaboration in [16] with the parameters they extracted from data. We used the helicity formalism of [24–26], to be consistent with the analysis in [16]. The COMPASS model

contains 88 partial waves. Each is a unique combination of quantum numbers for the three-pion state, a dynamic amplitude model for the two-pion isobar (denoted by ξ), and an orbital angular momentum between the isobar and the spectator pion. The three-pion quantum numbers are formulated in the reflectivity basis [27], with spin projection M and reflectivity ϵ . This is all abbreviated as $J^{PC} M^\epsilon \xi \pi L$.

Our πp -scattering fit model frees the dynamic amplitudes in eleven different waves distinguished by the quantum numbers of the three-pion system; the spin, j , of the two-pion isobar, which we write $[\pi\pi]_j$; and the angular momentum between the isobar and the spectator pion. These eleven freed waves, listed in table I, replace fifteen waves of the COMPASS model: waves with freed $[\pi\pi]_S$ replace those with the broad $\pi\pi$ S wave and the $f_0(980)$ (and $f_0(1500)$ in the 0^-+0^+ wave); waves with freed $[\pi\pi]_P$ replace those with the $\rho(770)$; and the wave with freed $[\pi\pi]_D$ replaces one with the $f_2(1270)$. The remaining 73 waves are included in their model-dependent formulation. Any combination of model-independent and model-dependent waves is possible within the freed-isobar approach; here we have freed the most prominent waves. The two-pion mass bins in each freed wave are contiguous and cover the full mass range from $2m_\pi$ to $m_{3\pi} - m_\pi$; near the regions of the $\rho(770)$ and $f_2(1270)$, they are 20 MeV wide; near the $f_0(980)$, they are 10 MeV wide; and elsewhere they are 40 MeV wide.

$J^{PC} M^\epsilon$	$[\pi\pi]_j \pi L$	
0^-+0^+	$[\pi\pi]_S \pi S, [\pi\pi]_P \pi P$	✓
$1^{++}0^+$	$[\pi\pi]_S \pi P, [\pi\pi]_P \pi S$	✓
$1^{++}1^+$	$[\pi\pi]_P \pi S$	
2^-+0^+	$[\pi\pi]_S \pi D, [\pi\pi]_P \pi P, [\pi\pi]_P \pi F, [\pi\pi]_D \pi S$	✓
2^-+1^+	$[\pi\pi]_P \pi P,$	
$2^{++}1^+$	$[\pi\pi]_P \pi D,$	

TABLE I: Freed waves in $\pi^- p \rightarrow \pi^- \pi^+ \pi^- p$, grouped by three-pion quantum numbers, with presence of a zero mode indicated in the last column.

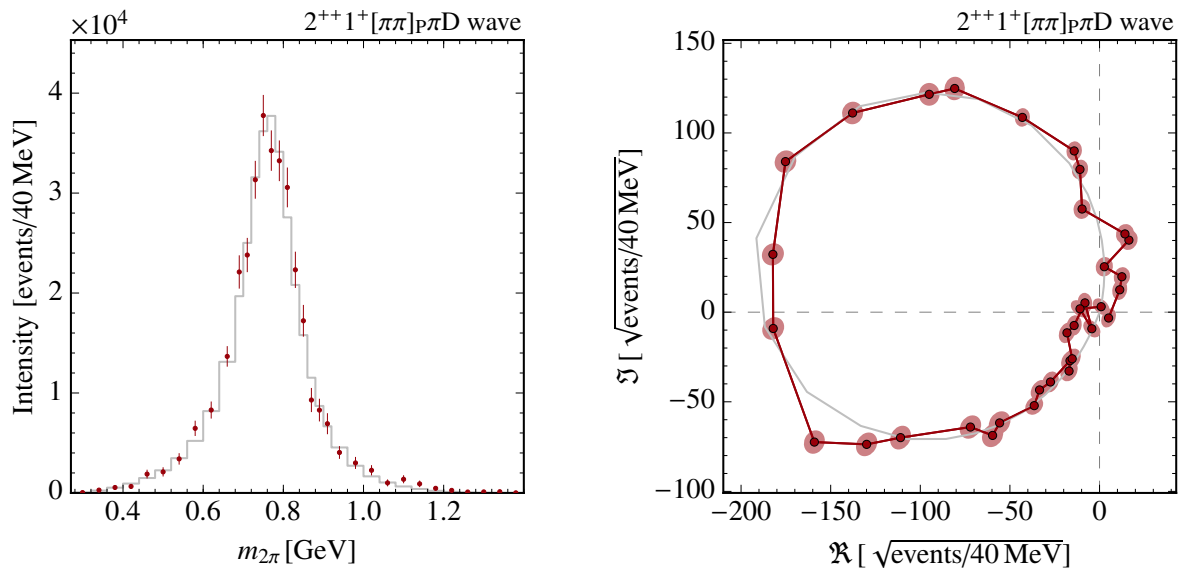


FIG. 3: Intensity (left) and dynamic amplitude in the complex plane (right) of the simulated π p-scattering model (grey) and the results of the fit to data (red).

Using the technique described in section III B, we find the zero modes of this scattering fit model. They do not connect waves with differing initial-state quantum numbers. We find three zero modes in this model—they are indicated in table I; each has one complex degree of freedom.

Figure 3 shows an example result from fitting this model to simulated data. The fit result is shown in red and the generating model in gray. The left plot shows the intensity as a function of two-pion mass; and the right plot shows the dynamic amplitude in the complex plane. All other plots in this section are identically structured. The freed-isobar shown is that of the $2^{++}1^+[\pi\pi]_P \pi D$ wave, which has no zero mode. The fit result agrees well with the data-generation model.

1. Complete-model constraint

With our freed D-decay model, we determine the complex dynamic amplitude value in each two-pion mass bin via a fit to simulated data. In figure 4, the red points show the fit results of the freed S and P waves. The grey lines show the data-generation model. The fit result has peaks corresponding to those of the generating model, but also considerable intensity elsewhere that does not match the generating model.

To correct for the zero mode, we fit for its complex parameter, $\tilde{\eta}$, by minimizing the χ^2 of equation (24). We predict ϵ_β^a in all bins of both the S and P waves using a model that contains both the $f_0(980)$ and $\rho(770)$ —that is, our original data-generation model. However, for our prediction we change the masses and widths of the resonances: for the $f_0(980)$, we shift the mass from 980 MeV

to 1 GeV and the width from 100 MeV to 110 MeV; for the $\rho(770)$, we shift the mass from 770 MeV to 750 MeV and the width from 160 MeV to 180 MeV.

In figure 4, the green points show the freed waves with the zero mode subtracted given the value of $\tilde{\eta}$ found in the second fit:

$$\alpha_\beta^a = \omega_\beta^a - \tilde{\eta} z_\beta^a. \quad (25)$$

This result very closely resembles the generating model. Though we predicted the ϵ_β^a with shifted values for the masses and widths, our final result recovers the correct values. This demonstrates that we do not need detailed and accurate expectations for the zero-mode correction; nor can we coax a result out of the fit via our expectation. This is in contrast to model-dependent PWA, which is very sensitive to the fit model. However, though our expectations for the zero-mode correction need not be detailed or accurate, they must still be reasonable: We must predict a feature that the data in some rough way contains. For example, we cannot predict ϵ_β^a from a model of a resonance for which our data is far below the threshold to produce since its features will be very weak in the data.

2. Partial-model constraint

With our freed π p-scattering model, we determine the complex dynamic amplitude value in each two-pion mass bin via a fit to simulated data. In figure 5, the red points show the fit results of the $0^{-+}0^+[\pi\pi]_S \pi S$ and $0^{-+}0^+[\pi\pi]_P \pi P$ freed waves. The grey lines show the data-generation model. The disagreement between the

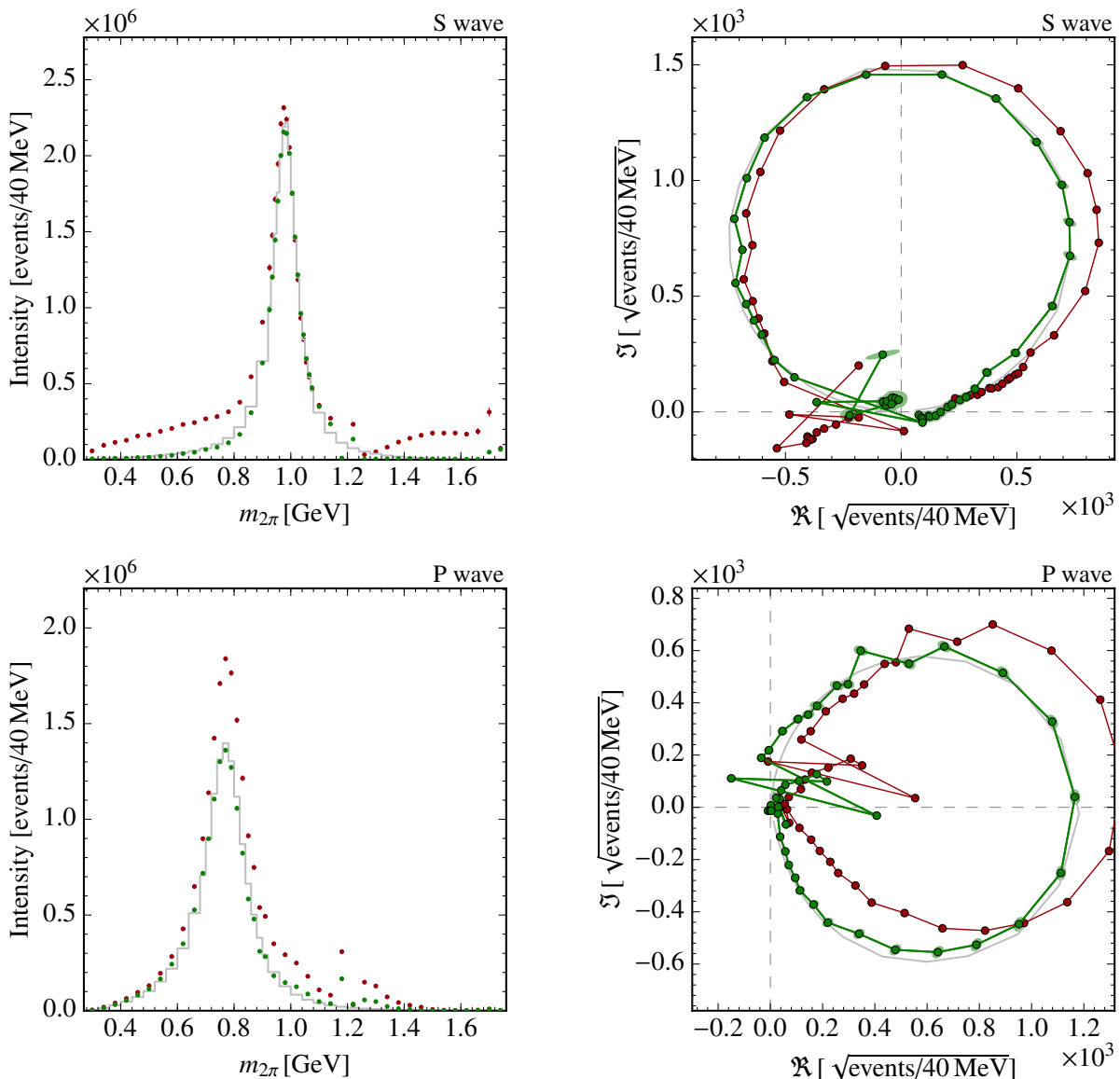


FIG. 4: Intensities (left) and dynamic amplitudes in the complex plane (right) of the simulated $D^- \rightarrow \pi^- \pi^+ \pi^-$ model (grey), the results of the fit to data (ω_β^a , red), and the results after zero-mode correction (α_β^a , green).

fit result and the generating model is due to the zero mode.

Again, to correct for the zero mode, we fit for its complex parameter, $\tilde{\eta}$, by minimizing χ^2 . Since the zero modes in our freed π p-scattering model are contained entirely in waves with the same initial-state quantum numbers, we need not assume a model for the entire process—which, with 84 partial waves, is very complicated—but only for the waves in which the zero mode arises. We need only predict ϵ_β^a for the relevant waves, and accordingly only sum over those waves in equation (24). In figure 5, the blue points show the freed waves with the zero mode subtracted given the value of $\tilde{\eta}$ found in the second fit. They agree well with the generating model.

Since the zero mode links the $[\pi\pi]_S \pi$ S wave and the

$[\pi\pi]_P \pi$ P wave, it is even enough to fit for $\tilde{\eta}$ in only one of them. We restrict our prediction of ϵ_β^a further to only the mass bins of the $[\pi\pi]_P \pi$ P wave, and accordingly sum only over those bins in equation (24). In figure 5, the green points show *both* freed waves with the zero mode subtracted given the value of $\tilde{\eta}$ found in a fit to *only* the P wave. The result very closely resembles the generating model and agrees well with the zero-mode correction that used both waves. This demonstrates that one can correct for a zero mode with only a minimal assumption about a model.

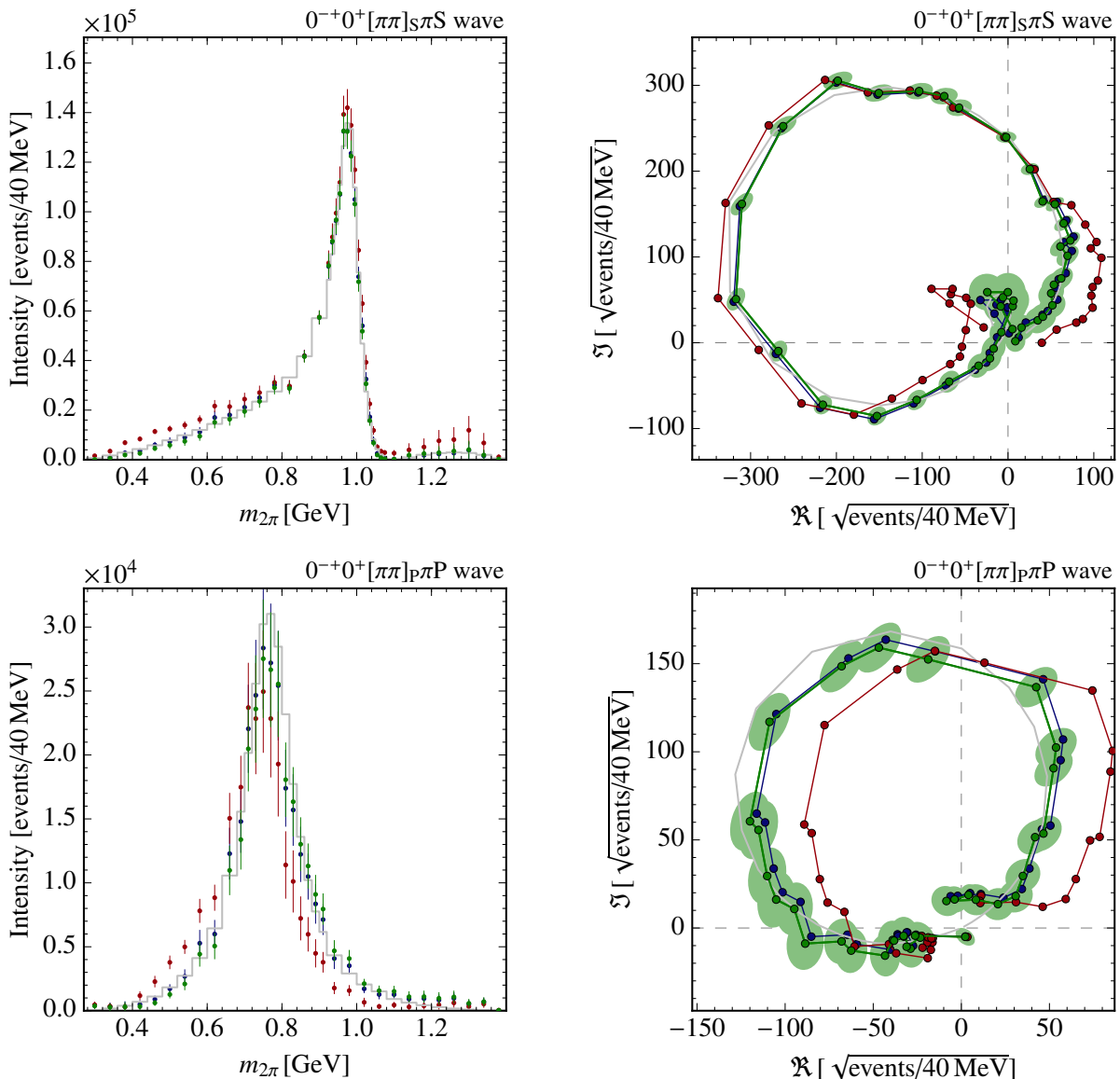


FIG. 5: Intensities (left) and dynamic amplitudes in the complex plane (right) of the simulated πp -scattering model (grey), the results of the fit to data (ω_β^a , red), and the results after zero-mode correction (α_β^a) using both the S and P waves (blue, without uncertainties) and using only the P wave (green).

3. Constraints with additional parameters

In both zero-mode corrections above, the only free parameters were the $\tilde{\eta}$. Additional parameters used to predict the ϵ_β^a , such as masses and widths of resonances in our assumed model, were fixed. But a common goal of PWA is to measure such parameters. It would be superfluous and error prone to first correct for the zero mode and then fit the zero-mode-corrected results for such parameters. Instead, we should fit for them and the contribution of the zero mode simultaneously.

We demonstrate this with a zero-mode-correction fit to the results in the $0^{-+}0^{+}[\pi\pi]_P \pi P$ wave of the πp -

scattering model (as determined, again, from a fit to simulated data). We fit for both $\tilde{\eta}$ and the mass and width of the $\rho(770)$ (in a Breit-Wigner lineshape) that is contained in this wave. We recover a zero-mode corrected result identical to that shown already in figure 5; and we find

$$m_\rho = (766.7 \pm 1.8) \text{ MeV} \quad (26)$$

$$\Gamma_\rho = (154.6 \pm 4.0) \text{ MeV}, \quad (27)$$

which agree within their uncertainties with the simulated values 769.0 MeV and 150.9 MeV.

V. CONCLUSION

Freed-isobar partial-wave analysis allows us to overcome the limits of model-dependent analysis by using empirical step functions to describe dynamic amplitudes. It can be useful for light-meson spectroscopy and analysis of heavy-meson decays and hadronic τ -lepton decays. In particular, for CP-asymmetry measurements, freed-isobar PWA could be a robust alternative to the common schemes of measuring asymmetries in bins of phase space. Using the technique, we could instead determine asymmetries in mass bins in distinct projections of the isobar quantum numbers.

Several analyses have used freed-isobar PWA in limited ways, both as a central analysis tool and as a cross check of model-dependent analyses. But more expanded use of the technique—to fit with many freed waves, whether initially or through a bootstrapping procedure—has failed to produce meaningful results. This is due to the presence of zero modes and their arbitrary degrees of freedom.

We have demonstrated how to correct for these zero modes and remove arbitrary degrees of freedom using minimal assumptions. And we have provided examples using simulated data of three-pion production via both pion-proton scattering and D-meson decay. Our enhanced freed-isobar PWA techniques may be useful for determining two-body dynamic amplitudes that are consistent across a large variety of strong-interaction problems; for example, one could test models of final-state interaction.

ACKNOWLEDGEMENTS

We acknowledge the support of the Cluster of Excellence Universe, Exc153, Computational Centre for Astro- and Particle Physics (C²PAP), Transregional Research Centre TR110, all funded by the Deutsche Forschungsgemeinschaft. We would like to thank M. Pennington (Sussex), A. Szepaniak (U. Indiana), J. Pelaez (Madrid), and W. Ochs (MPP) for many discussions in the course of this project.

Appendix A: Example Zero Modes

The solutions to equation 11—the zero modes—are dependent on the formalism chosen for ψ_a and are not guaranteed to exist for all scattering or decay processes. The zero modes are also dependent on the symmetrizations summed over—the presence (or lack thereof) of identical particles in the final state.

To demonstrate conditions under which zero modes appear, we consider, first, decay of a spinless meson to three spinless mesons, which is important for heavy-meson decay; and then give an example in decay of a spinful state.

1. Zero modes in decays of spinless mesons

Let us consider the decay

$$X \rightarrow h_1 h_2 h_3, \quad (\text{A1})$$

where all particles are spinless. For ψ_a , as in section III A, we use the Zemach tensor formalism. We limit our discussion to the S and P waves. Since the initial state is spinless, the spin of the resonance is always the same as the total orbital and spin angular momenta of the wave. Therefore there is only one wave for each isobar spin. For the decay to an isobar formed by ij with spin ℓ and a spectator final-state particle k (with i , j , and k standing for a cyclic permutation of h_1 , h_2 , and h_3), the spin-dependent amplitude is

$$\psi_{ij}^\ell(m_X, \vec{\tau}) = |\vec{p}_i|^\ell |\vec{p}_k|^\ell P_\ell(\hat{p}_i \cdot \hat{p}_k), \quad (\text{A2})$$

where P_ℓ is the ℓ 'th-order Legendre polynomial and the momenta are in the ij rest frame.

a. Zero modes purely in S waves

The S-wave spin-dependent amplitude is unity. Therefore the S-wave component of equation (11) is

$$\sum_a^{\hat{}} \tilde{\Delta}_a^S(\hat{m}). \quad (\text{A3})$$

We can compensate a constant complex pedestal in one S wave by subtracting that same constant complex pedestal from any other S wave. Therefore, if there is more than one S wave in the model, there are zero modes that link each pair of S waves. We can most simply represent this with a set of zero modes that are constant in each S wave,

$$\tilde{\Delta}_a^S(m) = \tilde{\beta}_a, \quad (\text{A4})$$

such that

$$\sum_a^{\hat{}} \tilde{\beta}_a = 0, \quad (\text{A5})$$

where the $\tilde{\beta}_a$ are complex variables, one per wave, each with two real degrees of freedom; for N_S independent S waves, there are $(N_S - 1)$ free arbitrary complex variables.

Such a zero mode arises, for example, in the decay $D^- \rightarrow K^+ K^- \pi^-$, in which there are two S waves: in $K^+ K^-$ and $K^+ \pi^-$. In contrast, no such zero mode arises in $D^- \rightarrow \pi^- \pi^+ \pi^-$ since there is only one S wave—in $\pi^+ \pi^-$ —with two symmetrizations. This illustrates the difference between symmetrizations—the swapping of identical final-state particles in and out of the isobar—and waves—different groupings of particle species into isobars. Different waves have independent dynamic amplitude; but different symmetrizations of a single wave share a single dynamic amplitude form.

b. Zero mode purely in P waves

The P-wave spin-dependent amplitude is

$$\psi_{ij}^{\text{P}}(\vec{\tau}) = \frac{1}{4} \left(m_{jk}^2 - m_{ik}^2 - (m_X^2 - m_k^2) \frac{m_i^2 - m_j^2}{m_{ij}^2} \right). \quad (\text{A6})$$

$$\frac{1}{4} \sum_{ijk} \left(\tilde{\Delta}_{ik}^{\text{P}}(m_{ik}) - \tilde{\Delta}_{jk}^{\text{P}}(m_{jk}) \right) m_{ij}^2 - (m_X^2 - m_k^2) \frac{m_i^2 - m_j^2}{m_{ij}^2} \tilde{\Delta}_{ij}^{\text{P}}(m_{ij}), \quad (\text{A7})$$

where the sum is over cyclic permutations of $h_1 h_2 h_3$ as ijk , and we have labeled each wave by the two final state particles forming its P-wave isobar. This amplitude is zero if all three isobar configurations are allowed and all dynamic amplitudes are

$$\Delta_a^{\text{P}}(m) = \tilde{\gamma} m^2, \quad (\text{A8})$$

with one arbitrary complex variable, $\tilde{\gamma}$, for all amplitudes.

Such a zero mode arises, for example, in the decay $D^0 \rightarrow \pi^+ \pi^- \pi^0$, in which all P-wave isobars are possible: $\pi^+ \pi^-$, $\pi^+ \pi^0$, and $\pi^- \pi^0$. No such zero mode arises in, for example, $D^- \rightarrow K^+ K^- \pi^-$, if we disallow an isobar in $K^- \pi^-$ because there are no doubly-charged mesons.

If two of the final-state particles are the same species and charge, as we have in the example decay $D^- \rightarrow \pi^- \pi^+ \pi^-$, there is no purely P-wave zero mode.

c. Zero modes connecting S and P waves

Let us extend the zero mode of equations (17) and (18) for the case of h_1 , h_2 , and h_3 each a unique particle species: The zero mode is constant in the P waves, but now each combination of final-state particles has an independent dynamic amplitude:

$$\tilde{\Delta}_{ij}^{\text{P}}(m) = 4\tilde{\eta}_{ij}. \quad (\text{A9})$$

Substituting this into equation (A7) gives the total P wave amplitude:

$$\sum_{ijk} (\tilde{\eta}_{ik} - \tilde{\eta}_{jk}) m_{ij}^2 - \tilde{\eta}_{ij} (m_X^2 - m_k^2) \frac{m_i^2 - m_j^2}{m_{ij}^2}, \quad (\text{A10})$$

where the sum, as above, is over cyclic permutations of $h_1 h_2 h_3$ as ijk . The summand is dependent on only one mass—the isobar mass. We can perfectly balance each term in the sum with S-wave dynamic amplitudes

$$\tilde{\Delta}_{ij}^{\text{S}}(m) = -(\tilde{\eta}_{ik} - \tilde{\eta}_{jk}) m^2 + \tilde{\eta}_{ij} (m_X^2 - m_k^2) \frac{m_i^2 - m_j^2}{m^2}, \quad (\text{A11})$$

If each final-state particles is unique, there is no symmetrization necessary and the P-wave component of equation (11) is

and get a total amplitude of zero. Such a zero mode arises if all S waves and any P wave are freed.

d. All zero modes in the S and P waves

If all S and P waves are freed, then the three different forms of zero mode demonstrated above are present:

$$\tilde{\Delta}_{ij}^{\text{S}}(m) = \tilde{\beta}_{ij} + (\tilde{\eta}_{jk} - \tilde{\eta}_{ik}) m^2 + \tilde{\eta}_{ij} (m_X^2 - m_k^2) \frac{m_i^2 - m_j^2}{m^2} \quad (\text{A12})$$

$$\tilde{\Delta}_{ij}^{\text{P}}(m) = 4\tilde{\eta}_{ij} + \tilde{\gamma} m^2, \quad (\text{A13})$$

There are seven arbitrary complex constants with one constraint: $\sum_{ij} \tilde{\beta}_{ij} = 0$. The combined shapes of all zero modes are complex functions that may contain phase motion that mimics a resonance. Figure 6 shows such a situation for the example decay $B^- \rightarrow D^0 K^- \pi^0$ with an example set of complex parameters for the zero mode. Large phase motion manifests in two of the waves—such a shape, if not corrected for, could lead to a wrong interpretation of an analysis result.

2. Further zero modes

Zero modes are seen in many other combinations of isobars beyond the above examples of spinless meson decays. One decay of particular interest is that of a 1^{+-} state into a 1^{--} isobar and a pseudoscalar meson in a relative P wave with two symmetrizations (as exists in our example final state, $\pi^- \pi^+ \pi^-$). We can write the amplitude using the relativistic tensor formalism of references [28–30] as

$$\left[\psi_{(ij)k}^{1^{+-}}(\vec{\tau}) \right]_{\mu} \propto \epsilon_{\mu\nu\rho\sigma} p_i^{\nu} p_j^{\rho} p_k^{\sigma}; \quad (\text{A14})$$

note, that this amplitude is a vector, since it describes a spin-one quantity. Because of the Levi-Civita tensor, ϵ ,

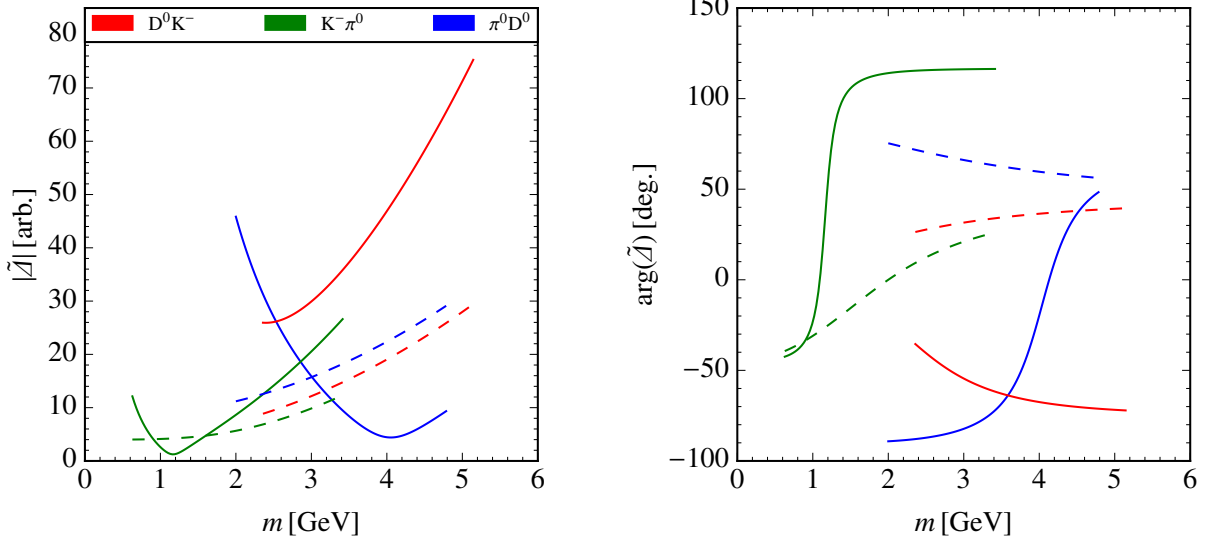


FIG. 6: S-wave (solid) and P-wave (dashed) dynamic components (magnitude, top; phase, bottom) of the generic zero mode in the decay $B^- \rightarrow D^0 K^- \pi^0$ with $\tilde{\eta}_{DK} = 1$, $\tilde{\eta}_{K\pi} = \exp(i45^\circ)$, and $\tilde{\eta}_{\pi D} = 2 \exp(i90^\circ)$; $\tilde{\beta}_{DK} = 1$, $\tilde{\beta}_{K\pi} = \exp(i120^\circ)$, and $\tilde{\beta}_{\pi D} = \exp(i240^\circ)$; and $\tilde{\gamma} = \exp(i45^\circ)$.

this changes sign under exchange of two indices. The symmetrized amplitude is therefore proportional to

$$\epsilon_{\mu\nu\rho\sigma} p_1^\nu p_2^\rho p_3^\sigma \left(\tilde{\Delta}(m_{12}) - \tilde{\Delta}(m_{23}) \right). \quad (\text{A15})$$

This is equal to zero everywhere if $\tilde{\Delta}(m) = \tilde{\Delta}(m')$ for all m and m' —that is, if $\tilde{\Delta}(m)$ is constant. Since $\tilde{\Delta}(m)$ may be complex, the zero mode has two degrees of freedom entirely contained in one isobar.

-
- [16] C. Adolph, R. Akhunzyanov, M. G. Alexeev, G. D. Alexeev, A. Amoroso, V. Andrieux, V. Anosov, W. Augustyniak, A. Austregesilo, C. D. R. Azevedo, et al. (COMPASS Collaboration), *Phys. Rev. D* **95**, 032004 (2017), URL <https://link.aps.org/doi/10.1103/PhysRevD.95.032004>.
- [17] E. M. Aitala, S. Amato, J. C. Anjos, J. A. Appel, D. Ashery, S. Banerjee, I. Bediaga, G. Blaylock, S. B. Bracker, P. R. Burchat, et al. (Fermilab E791 Collaboration), *Phys. Rev. D* **73**, 032004 (2006), URL <https://link.aps.org/doi/10.1103/PhysRevD.73.032004>.
- [18] J. Link, P. Yager, J. Anjos, I. Bediaga, C. Castromonte, A. Machado, J. Magnin, A. Massafferri, J. de Miranda, I. Pepe, et al., *Physics Letters B* **653**, 1 (2007), ISSN 0370-2693, URL <http://www.sciencedirect.com/science/article/pii/S0370269307007927>.
- [19] H.-X. Chen, W. Chen, X. Liu, and S.-L. Zhu, *Physics Reports* **639**, 1 (2016), ISSN 0370-1573, the hidden-charm pentaquark and tetraquark states, URL <http://www.sciencedirect.com/science/article/pii/S037015731630103X>.
- [20] D. J. Herndon, P. Söding, and R. J. Cashmore, *Phys. Rev. D* **11**, 3165 (1975), URL <https://link.aps.org/doi/10.1103/PhysRevD.11.3165>.
- [21] K. Gottfried and J. D. Jackson, *Il Nuovo Cimento* (1955-1965) **33**, 309 (1964), ISSN 1827-6121, URL <https://doi.org/10.1007/BF02750195>.
- [22] C. Zemach, *Phys. Rev.* **140**, B97 (1965), URL <https://link.aps.org/doi/10.1103/PhysRev.140.B97>.
- [23] G. Breit and E. Wigner, *Phys. Rev.* **49**, 519 (1936), URL <https://link.aps.org/doi/10.1103/PhysRev.49.519>.
- [24] M. Jacob and G. Wick, *Annals of Physics* **7**, 404 (1959), ISSN 0003-4916, URL <http://www.sciencedirect.com/science/article/pii/000349165990051X>.
- [25] S. U. Chung, *Phys. Rev. D* **48**, 1225 (1993), URL <https://link.aps.org/doi/10.1103/PhysRevD.48.1225>.
- [26] J. D. Richman (1984), URL <http://cds.cern.ch/record/153636/files/cer-000064884.pdf>.
- [27] S. U. Chung and T. L. Trueman, *Phys. Rev. D* **11**, 633 (1975), URL <https://link.aps.org/doi/10.1103/PhysRevD.11.633>.
- [28] A. V. Anisovich, V. V. Anisovich, V. N. Markov, M. A. Matveev, and A. V. Sarantsev, *Journal of Physics G: Nuclear and Particle Physics* **28**, 15 (2002), URL <http://stacks.iop.org/0954-3899/28/i=1/a=302>.
- [29] V. Filippini, A. Fontana, and A. Rotondi, *Phys. Rev. D* **51**, 2247 (1995), URL <https://link.aps.org/doi/10.1103/PhysRevD.51.2247>.
- [30] S. U. Chung, *Phys. Rev. D* **57**, 431 (1998), URL <https://link.aps.org/doi/10.1103/PhysRevD.57.431>.
- [16] C. Adolph, R. Akhunzyanov, M. G. Alexeev, G. D. Alexeev, A. Amoroso, V. Andrieux, V. Anosov, W. Augustyniak, A. Austregesilo, C. D. R. Azevedo, et al. (COMPASS Collaboration), *Phys. Rev. D* **95**,

- 032004 (2017), URL <https://link.aps.org/doi/10.1103/PhysRevD.95.032004>.
- [17] E. M. Aitala, S. Amato, J. C. Anjos, J. A. Appel, D. Ashery, S. Banerjee, I. Bediaga, G. Blaylock, S. B. Bracker, P. R. Burchat, et al. (Fermilab E791 Collaboration), *Phys. Rev. D* **73**, 032004 (2006), URL <https://link.aps.org/doi/10.1103/PhysRevD.73.032004>.
- [18] J. Link, P. Yager, J. Anjos, I. Bediaga, C. Castromonte, A. Machado, J. Magnin, A. Massafferri, J. de Miranda, I. Pepe, et al., *Physics Letters B* **653**, 1 (2007), ISSN 0370-2693, URL <http://www.sciencedirect.com/science/article/pii/S0370269307007927>.
- [19] H.-X. Chen, W. Chen, X. Liu, and S.-L. Zhu, *Physics Reports* **639**, 1 (2016), ISSN 0370-1573, the hidden-charm pentaquark and tetraquark states, URL <http://www.sciencedirect.com/science/article/pii/S037015731630103X>.
- [20] D. J. Herndon, P. Söding, and R. J. Cashmore, *Phys. Rev. D* **11**, 3165 (1975), URL <https://link.aps.org/doi/10.1103/PhysRevD.11.3165>.
- [21] K. Gottfried and J. D. Jackson, *Il Nuovo Cimento* (1955-1965) **33**, 309 (1964), ISSN 1827-6121, URL <https://doi.org/10.1007/BF02750195>.
- [22] C. Zemach, *Phys. Rev.* **140**, B97 (1965), URL <https://link.aps.org/doi/10.1103/PhysRev.140.B97>.
- [23] G. Breit and E. Wigner, *Phys. Rev.* **49**, 519 (1936), URL <https://link.aps.org/doi/10.1103/PhysRev.49.519>.
- [24] M. Jacob and G. Wick, *Annals of Physics* **7**, 404 (1959), ISSN 0003-4916, URL <http://www.sciencedirect.com/science/article/pii/000349165990051X>.
- [25] S. U. Chung, *Phys. Rev. D* **48**, 1225 (1993), URL <https://link.aps.org/doi/10.1103/PhysRevD.48.1225>.
- [26] J. D. Richman (1984), URL <http://cds.cern.ch/record/153636/files/ce-000064884.pdf>.
- [27] S. U. Chung and T. L. Trueman, *Phys. Rev. D* **11**, 633 (1975), URL <https://link.aps.org/doi/10.1103/PhysRevD.11.633>.
- [28] A. V. Anisovich, V. V. Anisovich, V. N. Markov, M. A. Matveev, and A. V. Sarantsev, *Journal of Physics G: Nuclear and Particle Physics* **28**, 15 (2002), URL <http://stacks.iop.org/0954-3899/28/i=1/a=302>.
- [29] V. Filippini, A. Fontana, and A. Rotondi, *Phys. Rev. D* **51**, 2247 (1995), URL <https://link.aps.org/doi/10.1103/PhysRevD.51.2247>.
- [30] S. U. Chung, *Phys. Rev. D* **57**, 431 (1998), URL <https://link.aps.org/doi/10.1103/PhysRevD.57.431>.